Jagannath University Journal of Science
Volume 10, Number II, Dec. 2023, pp. 145−158
https://jnu.ac.bd/journal/portal/archives/science.jsp
ISSN 3005-4486 (Online), ISSN 2224-1698 (Print)

Hydromagnetic Convective Heat Transfer in a Square Cavity Filled with Fe_3O_4-Water Nanofluid Saturated Porous Medium

Research Article

Md. Shariful Alam[1], Md. Nurul Huda[1,*] and S. M. Chapal Hossain[2]

[1]*Department of Mathematics, Jagannath University, Dhaka-1100, Bangladesh*

[2]*Department of Applied Mathematics, University of Dhaka, Dhaka-1000, Bangladesh*

DOI: https://doi.org/10.3329/jnujsci.v10i2.71266

Received: 2 October 2023, Accepted: 4 December 2023

ABSTRACT

A numerical study is carried out to demonstrate the heat transmission events of Fe_3O_4-H_2O nanofluid in a square cavity saturated by aluminum foam porous medium under the effect of slanted periodic magnetic field. The cavity wall is heated from left and cooled from right while horizontal walls are supposed to be adiabatic. The Brownian motion of nanoparticle is taken into consideration in the thermal conductivity model construction. The dimensionless governing equations including Darcy-Brinkman model are solved by Galerkin-FEM. The outcomes are exposed with depictions of streamlines, isotherms and average Nusselt numbers. The numerical investigation is performed for parameters: Darcy number, Rayleigh number, Hartmann number, porosity, leaning angle of the periodic magnetic field, period number, and nanoparticle volume fraction. The heat transfer rate upsurges noticeably for the rise of nanoparticle volume fraction, period number, Darcy number and Rayleigh number but the reverse trend is found for the parameter Hartmann number as well as porosity. From the acquired numerical outcomes, the maximum rate of heat transfer is attained at $Ha = 10$, $\delta = \pi/4$ when $\lambda = 1$.

Keywords: *Nanofluid, Brownian motion, Finite element method, Porous medium, Darcy-brinkman model*

1. Introduction

Heat transfer (HT) in conventional fluids (oil, ethylene glycol and water) have poor thermal conductivity (TC) that has limitation to enhance the thermal presentation and the compactness of various engineering electric instruments. Hence, in order to develop an advanced HT fluid, (Choi 1995) first introduced the concept of nanofluids (NFs) which have various engineering and industrial applications. The suspension of the solid

***Corresponding author:** Md. Nurul Huda
E-mail: mnurulhdu1@gmail.com

nanoparticles (NPs) into the conventional base fluids (BFs) significantly upsurges the TC and thus enhances the thermal performance characteristics. Due to many engineering applications, convective HT of nanofluids inside different shape of cavities have extensively studied by many researchers (Tiwari and Das 2007, Rahman et al. 2011, Celli 2013, Al Kalbani et al. 2016, Alam et al. 2022) worth mentioning.

Free convective HT and fluid in cavities occupied with NF-drenched porous medium (PM) performs an imperative part in numerous manufacturing uses including geothermal case, ground water contamination, thermal energy storing, crude oil extraction, flow via filtering medium, etc. Illustrative exploration in the field of PM can be originate in (Ingham and Pop 2005, Nield and Bejan 2013), etc. Due to the huge surface area, PM is appropriate as insulators and HT organizers in diverse engineering systems. Thus, competent use of such material desires a careful study for modeling energy and momentum transport. There are numerous momentum models for fluidic flow through a PM. The Darcy model, that accepts relationship between the pressure gradient and velocity, has been widely accustomed to inspect a number of fluid and HT cases with hot bodies attached in NF-drenched PM. This model is valid for weak flows over PM with poor permeability (Nakayama et al. 1990). For advanced flow rate or in highly PM, there is an exit case developed from the linear law and inertial effects. For a typical particle diameter, it revealed that the flow converts non-Darcian when the Reynolds number surpasses unity (Bear 1972). These departures are supposed to be due to flow separation inside the PM, while numerically creating itself as a nonlinear term in the velocity, pressure-gradient connection. (Muskat 1946) included a velocity and Forchheimer expressions to account for the PM inertia impacted on the pressure profiles, when (Brinkman 1947) a viscous diffusion term is pondered for the boundary frictional drag case.

Because of the importance of magnetic field (MF) on the flow field, several scholars (Al-Zamily 2014, Al Kalbani et al. 2016, and Sheikholeslami 2018) studied convective flow and HT of NF inside a cavity in the existence of a MF. The literature investigation linked to magnetohydrodynamic disclosures that a momentous number of researchers measured uniform MF effect in the flow field. However, the influences of oscillating MF on the natural convection (NC) flow in enclosures have received very little attention, though this occurrence seems in induction approach based magnetic pumps, and generators. (Turcotte and Lyons 2006) showed that for a high value of the MF interaction parameter, the oscillating MF limits the viscous forces inside the flow field. Besides, for the presence of a weak MF, the inertial boundary layer thickens the upstream flow direction. (Siddiqa et al. 2017) examined the effects of particles' micro-rotation behaviors during the macroscopic and microscopic level flows in the existence of a periodic MF. They informed that the HT rate is insensitive with the increase of the MF parameter. (Mehryan et al. 2018) studied influences of periodic MF on NC and entropy generation inside a quadrate cavity using ferrofluids. In their simulation, they noted that HT is advanced due to the oscillating MF linked to the uniform field regardless of the values of the *Ha* and the MF period.

Above mentioned literature shows that the natural convective HT and fluid flows in a four-sided cavity occupied with a PM saturated by a magnetic NF in the presence of inclined periodic MF using the NF models planned by (Tiwari and Das 2007, Celli 2013) has not been inspected so far. So, the aim of this study is to explore NC within a four-sided porous cavity adopted more accurate experimental correlations for the physical properties of the NFs (such as heat capacitance, TC and thermal diffusivity). The solid phase of the PM is set as AF. Particular exertions have been emphasized on the impacts of the Darcy number, the Rayleigh number, the solid VF factor, and the porosity of the PM on flow arena, temperature delivery, Nu, streamlines and isotherms.

2. Methods

2.1. Physical model description

An inclined periodic MF is attributed on an unsteady, incompressible, laminar, 2D convective

flow of Fe_3O_4-Water NF in a four-sided cavity saturated by aluminum foam porous medium of length L as publicized in Fig.1. We assume that the PM is homogeneous and isotropic. The four-sided cavity surfaces are measured as fixed and NC has been initiated by making temperature variances between cold and heated surfaces. The inclined periodic MF depends on the *x* and *y* coordinate systems and this relation is stated as $B=B_0\sin[\frac{2\pi}{\lambda_0}(x\cos\delta+y\sin\delta)]$,where λ_0 the dimensional period, B_0 amplitude and δ the inclination angle of the inclined periodic MF respectively. The left wall of the cavity is uniformly heated at temperature $(T = T_h)$, whereas the right wall is cold at lower temperature $(T = T_c)$ and other two horizontal walls are adiabatic. The thermal equilibrium case exists among the BF, nanoparticles and porous medium, and no slip case occurs among them. In the thermal radiation of flow domain, viscous dissipation and any chemical reactions are ignored. The gravitational acceleration *g* acts in the downwards direction and the Brownian motion (BM) effects are included in the flow domain. All side walls are taken to be rigid walls.

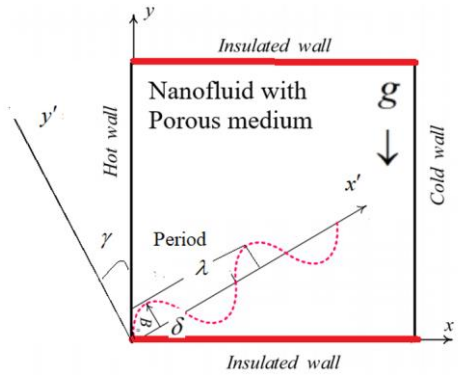

Fig.1: Physical geometry.

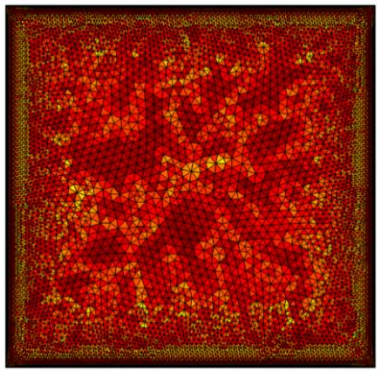

Fig. 2: Mesh geometry including 6282 elements.

Table-1. Thermal properties of the BF, nanoparticle and porous matrix (Sheremet et al. 2015, Alam et al. 2022)

BF/ Nanoparticle/ Porous matrix	c_p (J/kgK)	ρ (kg/m^3)	k (W/mK)	$\beta\times10^{-5}$ $(1/K)$	μ (Ns/m^2)	σ (S/m)	Pr
Water	4179	997.1	0.613	21	0.001003	5.5×10^{-6}	6.837
Aluminum foam (AF)	897	2700	205	-	-	-	-
Fe_3O_4	670	5180	80.4	20.6	-	0.112×10^{6}	-

2.2. Mathematical model

Based on the above stated directions and taking into attention the Darcy-Brinkman model for transport phenomena in PM, the dimensional governing equations are as follows (see also Nield and Bejan 2013, Al-Waheibi et al. 2021):

Continuity equation:

$$\frac{\partial u}{\partial x}+\frac{\partial v}{\partial y}=0 \qquad (1)$$

Momentum equations:

$$0 = -\frac{\partial p}{\partial x} - \frac{\mu_{nf}}{K}u + \frac{\mu_{nf}}{\varepsilon}\left(\frac{\partial^2 u}{\partial x^2} + \frac{\partial^2 u}{\partial y^2}\right) \tag{2}$$

$$-\frac{\sigma_{nf} B_0^2}{\rho_{nf}} \sin^2[\tfrac{2\pi}{\lambda_0}\left(x\cos\delta + y\sin\delta\right)](u\sin^2\delta - v\sin\delta\cos\delta)$$

$$0 = -\frac{\partial p}{\partial y} - \frac{\mu_{nf}}{K}v + \frac{\mu_{nf}}{\varepsilon}\left(\frac{\partial^2 v}{\partial x^2} + \frac{\partial^2 v}{\partial y^2}\right) + g\left(\rho\beta\right)_{nf}\left(T - T_C\right)$$

$$-\frac{\sigma_{nf} B_0^2}{\rho_{nf}} \sin^2[\tfrac{2\pi}{\lambda_0}(x\cos\delta + y\sin\delta)]\left(v\cos^2\delta - u\sin\delta\cos\delta\right) \tag{3}$$

Energy equation:

$$(\rho c_p)_m \frac{\partial T}{\partial t} + (\rho c_p)_{nf}\left(u\frac{\partial T}{\partial x} + v\frac{\partial T}{\partial y}\right) = \kappa_m\left(\frac{\partial^2 T}{\partial x^2} + \frac{\partial^2 T}{\partial y^2}\right) \tag{4}$$

2.3. Initial and Boundary conditions

For $t = 0$,

whole domain: $u = 0, v = 0, T = T_c, p = 0$ (5a)

For $t > 0$,

At the left hot wall: $u = 0, v = 0, T = T_h$ (5b)

At the top and bottom insulated walls: $u = 0, v = 0, \dfrac{\partial T}{\partial y} = 0$ (5c)

At the right cold wall: $u = 0, v = 0, T = T_c$ (5d)

2.4. Thermal and physical properties

For the present problem, effective heat conductance, effective thermal conductivity, viscosity, density, thermal diffusivity, heat capacitance, electrical conductivity, thermal expansion coefficient and thermal conductivity of nanofluid have been taken into consideration respectively as follows (see Rahman et al. 2021):

$$(\rho c_p)_m = (1-\varepsilon)(\rho c_p)_s + \varepsilon(\rho c_p)_{nf} \tag{6}$$

$$\kappa_m = (1-\varepsilon)\kappa_s + \varepsilon\kappa_{nf} \tag{7}$$

$$\mu_{nf} = \frac{\mu_{bf}}{(1-\phi)^{2.5}} \tag{8}$$

$$\rho_{nf} = \rho_{sp}\phi + (1-\phi)\rho_{bf} \tag{9}$$

$$\alpha_{nf} = \frac{\kappa_{nf}}{(\rho C_p)_{nf}} \tag{10}$$

$$(\rho c_p)_{nf} = \phi(\rho c_p)_{sp} + (1-\phi)(\rho c_p)_{bf} \tag{11}$$

$$\sigma_{nf} = \sigma_{bf}\frac{\sigma_p + 2\sigma_{bf} + 2(\sigma_p - \sigma_{bf})\phi}{(\sigma_p + 2\sigma_{bf}) - (\sigma_p - \sigma_{bf})\phi} \tag{12}$$

$$(\rho\beta)_{nf} = \phi(\rho\beta)_{sp} + (1-\phi)(\rho\beta)_{bf} \tag{13}$$

$$\kappa_{nf} = \kappa_{bf}\left[\frac{\kappa_{sp} + (n-1)\kappa_{bf} - (n-1)\phi\left(\kappa_{bf} - \kappa_{sp}\right)}{\kappa_{sp} + (n-1)\kappa_{bf} + \phi\left(\kappa_{bf} - \kappa_{sp}\right)}\right]$$

$$+\frac{(\rho c_p)_{sp}\phi}{2D_T^l}\sqrt{\frac{2D_T k_B T_{ref}}{3\pi\mu_{nf} d_p}} \tag{14}$$

where,

$D_T = 0.126\dfrac{\kappa_{nf}\beta_{bf}\mu_{nf}(0.0002d_p + 0.1537)}{\kappa_{bf}\rho_{nf}}$, $D_T^l = \sqrt{D_T}$ and T_{ref} is the reference temperature. In the above eq (14), the last term on the R.H.S. is due to the Brownian motion of the NPs. Brownian motion is a result of the collisions (due to random motion) of the NPs that are suspended in the BF and it is taken into the TC correlation in eq (14) which is related to eq (4) through eq (7).

All the symbols name and the interrelated quantities are given in the nomenclature.

2.5. Non-dimensional analysis

To describe numerous transport manifestations in NFs, the governing equations transformed into dimensionless form with help of the governing flow constraints. The following dimensionless governing equations (16)-(19) are created, accordingly, by including the dimensionless variables in (15) into the dimensional equations (1)-(4).

$$\left.\begin{aligned} X = \frac{x}{L},\ Y = \frac{y}{L},\ \mathrm{U} = \frac{uL}{\alpha_{bf}},\ \mathrm{V} = \frac{vL}{\alpha_{bf}},\ \mathrm{P} = \frac{pL^2}{\rho_{bf}\alpha_{bf}^2},\ \\ \theta = \frac{T - T_C}{T_h - T_C},\ \tau = \frac{t\alpha_{bf}}{L^2},\ \upsilon_{bf} = \frac{\mu_{bf}}{\rho_{bf}},\ \lambda = \frac{\lambda_0}{L},\ A = \frac{a}{L} \end{aligned}\right\} \tag{15}$$

$$\frac{\partial U}{\partial X}+\frac{\partial V}{\partial Y}=0 \tag{16}$$

$$0=-\frac{\partial P}{\partial X}-\frac{\mu_{nf}}{\mu_{bf}}\frac{\Pr}{Da}U+\frac{\mu_{nf}}{\mu_{bf}}\frac{\Pr}{\varepsilon}\left(\frac{\partial^2 U}{\partial X^2}+\frac{\partial^2 U}{\partial Y^2}\right) \tag{17}$$

$$-\Pr Ha^2\frac{\sigma_{nf}}{\sigma_{bf}}\sin^2[\tfrac{2\pi}{\lambda}(X\cos\delta+Y\sin\delta)]\left(U\sin^2\delta-V\cos\delta\sin\delta\right)$$

$$0=-\frac{\partial P}{\partial Y}-\frac{\mu_{nf}}{\mu_{bf}}\frac{\Pr}{Da}V+\frac{\mu_{nf}}{\mu_{bf}}\frac{\Pr}{\varepsilon}\left(\frac{\partial^2 V}{\partial X^2}+\frac{\partial^2 V}{\partial Y^2}\right)+\frac{(\rho\beta)_{nf}}{(\rho\beta)_{bf}}Ra\Pr\theta \tag{18}$$

$$-\Pr Ha^2\frac{\sigma_{nf}}{\sigma_{bf}}\sin^2[\tfrac{2\pi}{\lambda}(X\cos\delta+Y\sin\delta)]\left(V\cos^2\delta-U\cos\delta\sin\delta\right)$$

$$A_1\frac{\partial\theta}{\partial\tau}+U\frac{\partial\theta}{\partial X}+V\frac{\partial\theta}{\partial Y}=B_1\left(\frac{\partial^2\theta}{\partial X^2}+\frac{\partial^2\theta}{\partial Y^2}\right) \tag{19}$$

where, $A_1=(1-\varepsilon)\gamma+\varepsilon$, $B_1=\dfrac{1-\varepsilon}{\xi}\delta_1+\dfrac{\varepsilon\kappa_{nf}}{\xi\kappa_{bf}}$,

$$\gamma=\frac{(\rho c_p)_s}{(\rho c_p)_{nf}},\ \xi=\frac{(\rho c_p)_{nf}}{(\rho c_p)_{bf}},\ \delta_1=\frac{\kappa_s}{\kappa_{bf}},\ \Pr=\frac{\upsilon_{bf}}{\alpha_{bf}},$$

$$Ra=\frac{g\beta_{bf}\left(T_h-T_c\right)L^3}{\alpha_{bf}\upsilon_{bf}},\ Ha=B_0L\sqrt{\frac{\sigma_{bf}}{\mu_{bf}}},\ Da=\frac{K}{L^2}.$$

For $\tau=0, U=0, V=0, \theta=0, P=0$ (20a)

For $\tau>0$, the dimensionless boundary settings (5b) - (5d) become,

At the left hot wall: $U=0, V=0, \theta=1$ (20b)

At the top and bottom insulated walls: $U=0, V=0, \dfrac{\partial\theta}{\partial Y}=0$ (20c)

At the right cold wall: $U=0, V=0, \theta=0$ (20d)

3. Heat transfer parameters

The dimensionless version of the convective HT coefficient is known as the Nusselt number (Nu), which is introduced by German engineer Wilhelm Nusselt (1882-1957). The HT rate is evaluated by the local and average Nu at the left heated wall that are evaluated as follows:

The local Nu on the heated wall can be written as

$$Nu_L=-\frac{\kappa_{nf}}{\kappa_{bf}}\left(\frac{\partial\theta}{\partial X}\right)_{X=0} \tag{21a}$$

The average Nu at the heated wall can be written as

$$Nu_{ave}=\int_0^1 Nu_L\,dY \tag{21b}$$

4.1. Numerical methodology

The dimensionless transport equations (16)-(19) with the boundary settings (20a) - (20d) are elucidated numerically by using Galerkin-FEM. The particulars of this technique can be found in the former reports (Rahman et al. 2009, 2011; Zienkiewicz and Taylor 1991). Briefly, the entire solution domain is discretized into non-uniform triangular shape finite element meshes. Six node triangular shape elements are chosen to formulate the finite element equations. All six nodes are allied with velocities, and temperature; the corner nodes are related with pressure. A lower order polynomial is selected for pressure, which is satisfied through the continuity equation. Then the nonlinear model equations are shifted into a system of integral equations by applying Galerkin weighted residual technique. The integration involved in each term of these equations is performed by using Gauss's quadrature technique. The resultant algebraic equations are improved by imposition of boundary conditions. To solve the set of the universal algebraic equations in the form of matrix, the N-R iteration procedure has been adapted through PDE solver with In-house code. The convergence criterion of the numerical solutions along with error guesstimate has been set to be $\left|\mathrm{I}^{m+1}-\mathrm{I}^{m}\right|\le 10^{-5}$, where $I\in\{U,V,\theta\}$ and m is the iteration number.

4.2. Grid statistics

To fix the suitable grid size, a grid independent examination is guided taking $\phi=0.02, Ha=10,$

$Da=10^{-3}, \varepsilon=0.8, Ra=10^6, \delta=\frac{\pi}{6}, \lambda=0.10, d_p=10nm,$

$n=3, \tau=0.1, Pr=6.8377.$

Table-2. Grid information for Fe_3O_4-H_2O nanofluid with AF porous medium.

Mesh name	Fine	Finer	Extra Fine	Extremely Fine
No. of Elements	928	1856	6282	24912
No. of Nodes	503	983	3242	12657
Nu_{ave}	110.38	110.51	110.61	110.62

In the current work, four dissimilar non-uniform grid systems with the total number of elements inside the flow field: 928, 1856, 6282 and 24912 are scrutinized. The numerical design is assembled for extremely precise key in the Nu_{ave} for the aforementioned elements to mature an understanding of the grid fineness as found in Table-2. The Nu_{ave} for 6282 elements demonstration a very small variance with the outcomes found for the 24912 elements. So, the grid size of 6282 and 24912 elements is adopted to obtain the precise outcomes. In this current study, herein chosen 6282 triangular elements to solve the nanofluid flow model for the well convergent solution.

4.3. Code justification

This current model has been authenticated in the absence of NPs, and this study is constrained to the study of water in a four-sided porous cavity for steady-state natural convection with isothermal vertical and insulated horizontal walls. Thus, to check the legitimacy of this current technique and code, the computed Nu_{ave} for three different values of Rayleigh numbers have been shown in Table-3 for some relative data with those described by (Walker and Homsy 1979, Manole and Lage 1992, Baytas and Pop 1999, Sheremet et al. 2015). These validations encouraging the sureness in the numerical result of our current study.

Table-3. Comparison of the Nu_{ave} at the left heated wall.

Authors	$Ra = 10^2$	Error (%)	$Ra = 10^3$	Error (%)	$Ra = 10^4$	Error (%)
Walker and Homsy (1979)	3.097	0.71	12.96	7.77	51.0	3.97
Manole and Lage (1992)	3.118	0.03	13.637	2.42	48.117	1.78
Baytas and Pop (1999)	3.16	1.29	14.06	0.66	48.33	1.33
Sheremet et al. (2015)	3.115	0.13	13.667	2.19	48.823	0.31
Present results	3.119		13.967		48.972	

5. Results and discussion

This section, the gotten outcomes are scrutinized to inspect the effects of slanted periodic MF strength of the square cavity filled with Fe_3O_4-H_2O NF with AF porous medium having uniform thermal boundary condition at the left heated wall. Thus, for Fe_3O_4-Water NF and AF porous medium, the values of heat capacitance ratios and TC ratios are calculated as $\gamma = 0.58318$, $\xi = 0.99666$ and $\delta_1 = 334.42$ with these calculated results and for porosity $\varepsilon = 0.8$, the values of $A_1 = 0.91664$, and $B_1 = 68.374$ have been picked into the numerical simulation for Fe_3O_4-H_2O NF. Calculations are made for various values of the pertinent parameters including periodic MF inclination angle, period of the MF, Darcy number, Rayleigh number, NP VF, and porosity of the PM on flow and thermal field. The outcomes are displayed in the form of streamlines and isotherms decorations to display the flow and thermal arenas. Furthermore, the variant of Nu_{ave} at the left heated wall for different model parameters is also decorated in line graphs as

well as tabular form. The main focus of the results is to obtain a clear idea of the HT regarding Fe_3O_4-H_2O nanofluid with AF porous medium filled square cavity for industrial uses.

Fig.3a and Fig. 3b respectively display the streamlines, and isotherms evolutions for different values of τ for AF porous medium, when $Da = 0.001, \phi = 0.02, \varepsilon = 0.8,\ Ha = 10,\ Ra = 10^6,$ $\lambda = 0.10, \delta = \frac{\pi}{6}, n = 3, d_p = 10nm.$ From Fig.3a and Fig.3b, it is observed that when $\tau = 0.1$, there are no significant changes in the streamlines and isotherms for $\tau > 0.1$, which means that the solution reaches to the steady state.

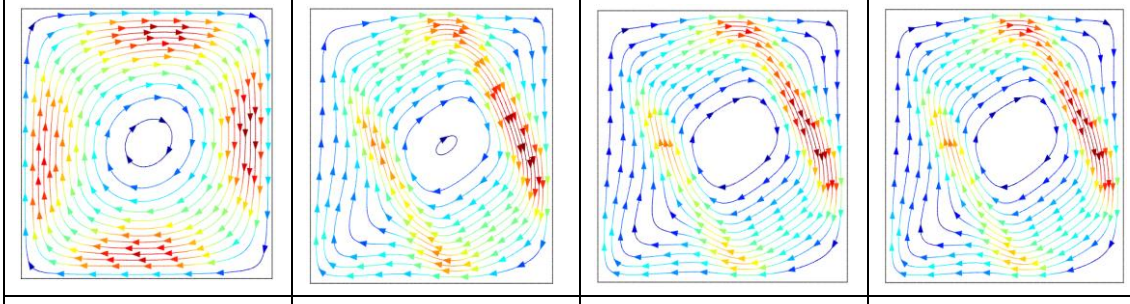

$\tau = 0.01$	$\tau = 0.08$	$\tau = 0.1$	$\tau = 0.2$

Fig. 3a. Streamlines evolutions for different values of τ for AF porous medium, when $\phi = 0.02$, $Ra = 10^6$, $Da = 0.001, \lambda = 0.10, \delta = \frac{\pi}{6}, n = 3, \varepsilon = 0.8, d_p = 10nm,\ Ha = 10.$

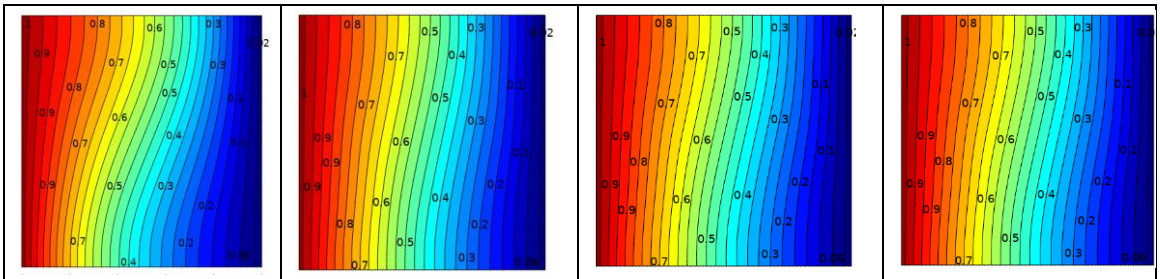

$\tau = 0.01$	$\tau = 0.08$	$\tau = 0.1$	$\tau = 0.2$

Fig. 3b: Isotherms evolutions for different values of τ for AF porous medium, when $\phi = 0.02$, $Ra = 10^6$, $Da = 0.001, \lambda = 0.10, \delta = \frac{\pi}{6}, n = 3, \varepsilon = 0.8, d_p = 10nm,\ Ha = 10.$

The joint effects of *Ha* and *Da* for $Ha=1,10,30; Da=10^{-4}, 10^{-3}, 10^{-2}$ on the streamlines and isotherms are presented in Fig.4a and 4b, respectively. There seems one big clockwise rotating vortex within the enclosure for all the cases. But they look scrawny and weak. The eye of revolutions is positioned near the center of each. The buoyancy-driven rotating flows inside the cavity are obvious for all values of the *Ha* and *Da*. The streamlines are distorted meaningfully indicating a weak buoyancy driven flow. It is also gotten that the strength and compactness of the streamlines are augmented with the increment of *Da*. But the strength and compactness of the streamlines are decreased very slow with the increment of *Ha*. To show the physical insight of the fluid flow rotation more precisely, it is imperative to evaluate the optimum surface velocity, as it specifies the flow circulation within

Ha	$Da=10^{-4}$	$Da=10^{-3}$	$Da=10^{-2}$
1	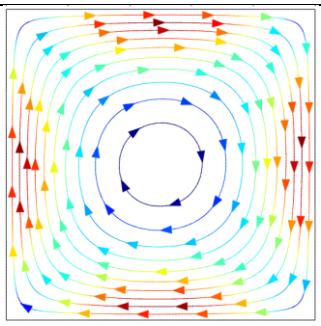	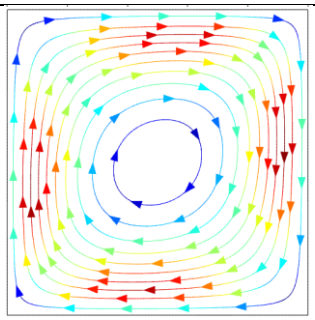	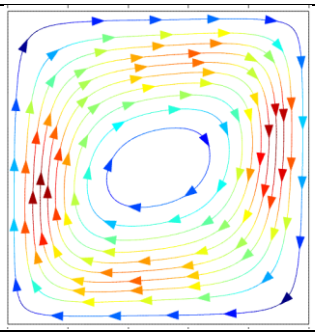
	$(U,V)_{max}$ = (30.363,30.236)	$(U,V)_{max}$ = (231.70,233.85)	$(U,V)_{max}$ = (791.11,890.86)
10	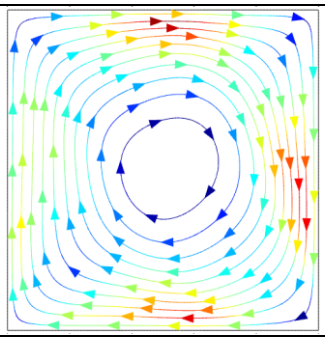	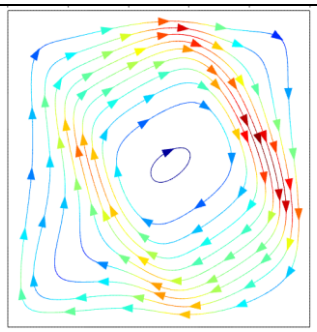	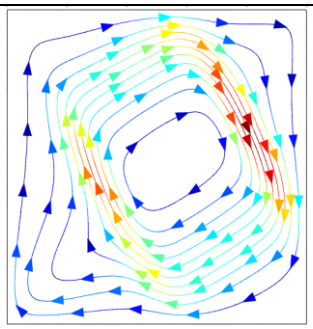
	$(U,V)_{max}$ = (28.909,21.386)	$(U,V)_{max}$ = (156.66,132.47)	$(U,V)_{max}$ = (304.97,341.81)
30	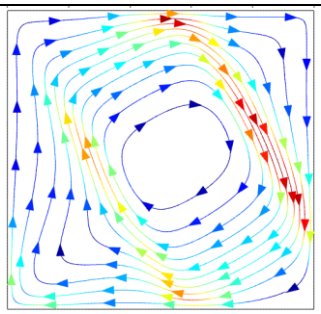	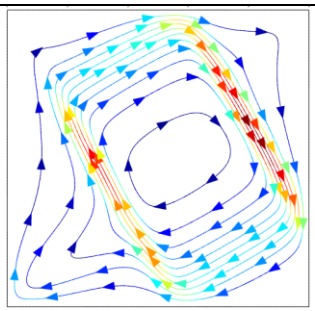	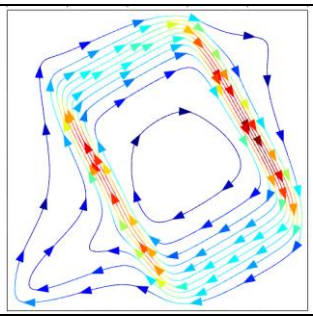
	$(U,V)_{max}$ = (23.151,17.267)	$(U,V)_{max}$ = (76.570,88.958)	$(U,V)_{max}$ = (108.27,133.91)

Fig.4a: Streamlines for different values of $Ha \& Da$ for AF porous medium, when $\phi = 0.02, \varepsilon = 0.8,$ $Ra = 10^6,\ \lambda = 0.10, \delta = \frac{\pi}{6}, n = 3, d_p = 10nm, \tau = 0.1.$

the cavity. So, we have evaluated the optimum surface velocity *(U, V)* for all the cases. It is obvious from the figures that the highest values of the optimum surface velocity is $(U,V)_{max}$ = (791.11, 890.86) which is obtained for *Ha =1* and $Da = 10^{-2}$.

The isothermal contours of *Ha* and different *Da* are presented in Fig. 4b. The *Ha* shows very low effect on the isotherms. Figure shows that isotherms are closer to one another nearby the hot surface of the enclosure. So, the temperature difference at the enclosure near the heated wall is greater than cold

Ha	$Da=10^{-4}$	$Da=10^{-3}$	$Da=10^{-2}$
1	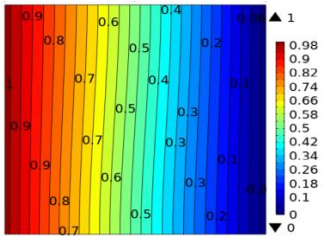	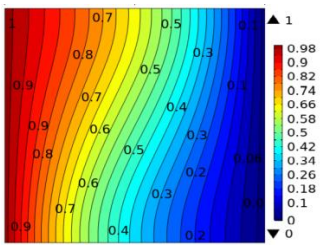	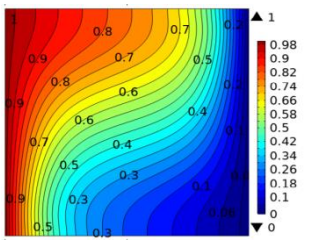
10	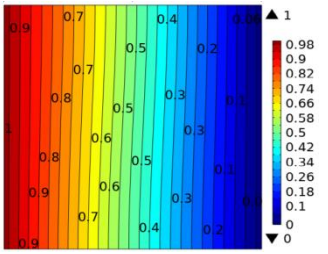	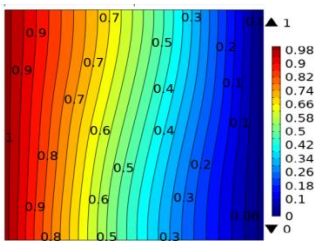	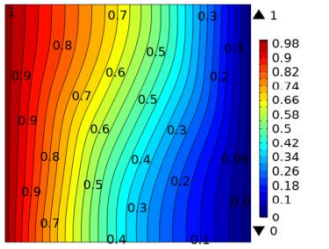
30	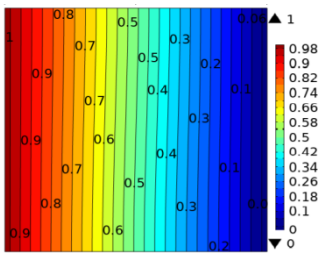	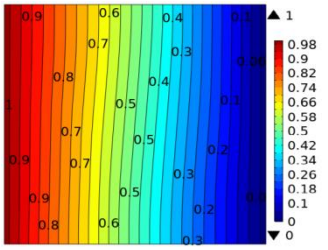	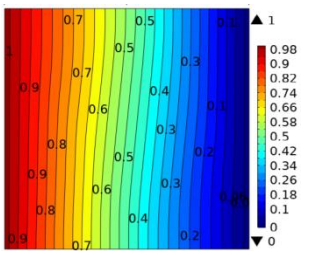

Fig.4b: Isotherms for dissimilar values of Ha & Da for AF porous medium, when $\phi=0.02, Ra=10^6,\ \lambda=0.10, \delta=\frac{\pi}{6}, n=3, \varepsilon=0.8, d_p=10nm, \tau=0.1.$

wall, which reproduces higher HT at the left partition of the cavity. For $Da=10^{-4}$ and as the *Ha* rises the isotherms lines are converted to parallel each other, which is a clear sign that convection to conduction as the mode of HT. Behavior of isotherms for *Ha* are almost similar, whereas for $Da=10^{-3},10^{-2}$ behave differently and the convection is the dominant mode of HT.

The distribution of Nu_{ave} versus the *Ha* for dissimilar values of *Da* along the left heated wall are displayed in Fig.5a, when $Ra=10^6,\ \phi=0.02,$ $\delta=\frac{\pi}{6}, d_p=10nm,\ \varepsilon=0.8, \lambda=0.10,\ n=3,\ \tau=0.1.$ From this figure we perceive that the Nu_{ave} rises with the increment of the *Da* and decreases with the increment of the *Ha*. A high *Da* corresponds to a strong buoyancy force that means providing more thermal energy to the system. So, the HT rate from the left heated wall to the cavity upsurges. We can say that both the *Ha* and the *Da* play a momentous role on the HT analysis. The distribution of Nu_{ave} versus the *Ha* for dissimilar values of ε along the left heated wall are displayed in Fig.5b, when $\lambda=0.10,$

$Ra=10^6, \phi=0.02, Da=10^{-3}, d_p=10nm,\quad \delta=\frac{\pi}{6},$ $n=3, \tau=0.1.$ From this figure we observe that the Nu_{ave} decreases with the augmentation of ε and *Ha*. So, the HT rate from the left heated surface to

the cavity decreases. we can say that both the *Ha* and the ε play a noteworthy role on the HT analysis. From the definition of *Ha*, we see that it represents the ratio of magnetic force (Lorentz force) to viscous force. Thus, for advanced values of *Ha* (*Ha*>50 for the present study) indicates higher values of Lorentz force that slow down

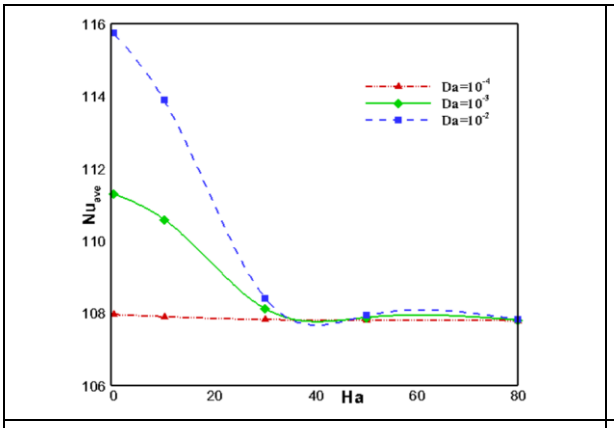

Fig. 5a. Distribution of Nu_{ave} versus *Ha* , *Da*.

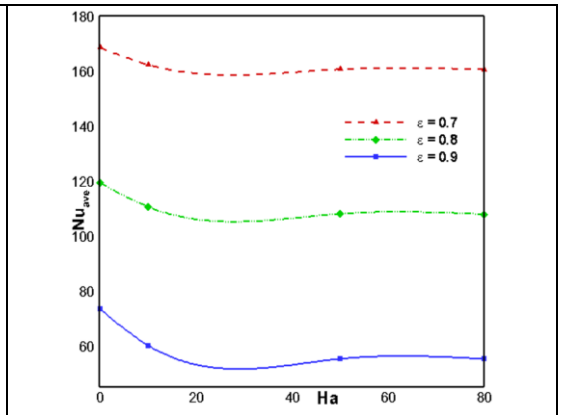

Fig. 5b. Distribution of Nu_{ave} versus *Ha*, ε .

the velocity of the NF within the cavity. Consequently, conduction mode of HT is dominant for *Ha*>50 whereas the convection mode of HT is dominant for *Ha*<50 as observed in Figs. 5a and Fig. 5b.

Table-4, illustrates the variation of Nu_{ave} along left heated wall for the combined effects of δ and λ for dissimilar values of *Ha*. From this table it is evident that the Nu_{ave} and HT rate diminutions with the upsurge in *Ha*. Moreover, Nu_{ave} rises with the growing value of λ and strongly depends on the δ . This means that the variation of the Nu_{ave} in terms of λ and δ changes by MF orientation. It is also noticed from this table that the highest thermal performance is achieved at an inclination angle $\delta = \frac{\pi}{4}, \lambda = 1$ and *Ha*=10. Therefore, we may say that both the inclination angle as well as period of the MF play a momentous role on the HT analysis.

Table-4. Variation of Nu_{ave} on the left heated wall for dissimilar Ha,δ and λ when Ra=10^6, $\phi = 0.02, \varepsilon = 0.8, Da = 0.001, d_p = 10nm, \tau = 0.1.$

Ha	δ	Nu_{ave}				
		$\lambda = 0.10$	$\lambda = 0.25$	$\lambda = 0.50$	$\lambda = 0.75$	$\lambda = 1$
10	0	109.95	114.74	117.67	118.52	118.85
	$\frac{\pi}{6}$	110.60	115.41	117.97	118.67	118.94
	$\frac{\pi}{4}$	110.74	115.59	118.05	118.71	118.96
	$\frac{\pi}{3}$	110.69	115.46	117.99	118.68	118.94
	$\frac{\pi}{2}$	109.98	114.69	117.63	118.49	118.83

20	0	108.32	110.91	114.74	116.69	117.67
	$\frac{\pi}{6}$	108.58	111.65	115.41	117.14	117.97
	$\frac{\pi}{4}$	108.63	111.82	115.59	117.27	118.05
	$\frac{\pi}{3}$	108.63	111.74	115.46	117.17	117.99
	$\frac{\pi}{2}$	108.33	110.93	114.69	116.64	117.63
30	0	107.99	109.34	112.42	114.74	116.19
	$\frac{\pi}{6}$	108.11	109.89	113.21	115.41	116.71
	$\frac{\pi}{4}$	108.13	110.00	113.40	115.59	116.85
	$\frac{\pi}{3}$	108.13	109.97	113.28	115.46	116.74
	$\frac{\pi}{2}$	108.00	109.37	112.41	114.69	116.14

Table-5, illustrates the Nu_{ave} (with/without Brownian effect) along left heated surface for dissimilar values of Ra and ϕ, when $Ha = 10$, $\varepsilon = 0.8, Da = 10^{-3}, \delta = \frac{\pi}{6}, n = 3, \lambda = 0.10,\ d_p = 10nm,$ $\tau = 0.1.$ All the result so gotten are considering the BM effect on the nanofluid TC, κ_{nf} , as well-defined in eq.14. It is clear that the BM recognizes a remarkable part in augmentation of the temperature delivery rate. The input of BM is exposed the NPs activity within the neighborhood which is enhancement the fluid temperature and micro convection sorts. Thus, a comparison study is achieved for the increment of the Nu_{ave} and gotten from the tabular outcomes that the impact of ϕ on the Nu_{ave} more momentous for both cases with or without BM. For example, when BM is taken into consideration, the Nu_{ave} increases 59.36% at $Ra = 10^6$ with $\phi = 0.02$ and the Nu_{ave} increases 6.52% for the other case.

Table-5: Average Nusselt number (with/without Brownian effect) along left hot surface for dissimilar values of Ra and ϕ when $Ha = 10,\ d_p = 10nm, \lambda = 0.10,\ \varepsilon = 0.8,\ Da = 10^{-3}, \delta = \frac{\pi}{6},\ n = 3, \tau = 0.1.$

Ra	ϕ	Nu_{ave}			
		With Brownian effect	Increase (%)	Without Brownian effect	Increase (%)
10^4	0	67.684	-	67.684	-
	0.005	77.791	14.93	68.751	1.58
	0.01	87.844	29.79	69.830	3.17
	0.015	97.845	44.56	70.921	4.78
	0.02	107.79	59.25	72.024	6.41

10^5	0	67.701		67.701	
	0.005	77.811	14.93	68.768	1.58
	0.01	87.867	29.79	69.848	3.17
	0.015	97.870	44.56	70.939	4.78
	0.02	107.82	59.26	72.043	6.41
10^6	0	69.402	-	69.402	-
	0.005	79.781	14.95	70.515	1.60
	0.01	90.108	29.83	71.640	3.22
	0.015	100.38	44.64	72.777	4.86
	0.02	110.60	59.36	73.926	6.52

6. Conclusions

The analysis of NC transient flow of Fe_3O_4-H_2O nanofluid in a square shape cavity filled with AF PM having uniform thermal boundary settings in presence of inclined periodic MF has been inspected numerically for the accepting of HT approaches and rates. The results of thermo-fluid flow behaviors are displayed graphically with streamlines, isotherms and Nu_{ave}. The Nu_{ave} is displayed by tables and line graphs. Major findings are as follows:

1. The solution reaches to steady state for $\tau = 0.1$ in the present investigated Darcy-Brinkman mathematical nanofluid model.
2. For $Ha = 1$ and $Da = 10^{-2}$, surface velocities are maximum, indicates strong flow of NF inside the cavity.
3. Conduction is the approach of HT for lower value of Da and higher value of Ha.
4. The Nu_{ave} of Fe_3O_4-H_2O NF rises significantly for the upsurge of NP volume fraction, period number, *Da* and *Ra*.
5. The Nu_{ave} of Fe_3O_4-H_2O NF due to the augmentation of MF leaning angle is not monotonic.
6. As magnetic field parameter *Ha* as well as porosity decrease, Nu_{ave} increases remarkably.
7. The highest rate of HT is achieved at Hartmann number $Ha = 10$, MF inclination angle $\delta = \pi / 4$ when period number λ =1.
8. When BM of the NPs is taken into discretion of the thermal conductivity model, the HT rate is increased 59.36% at $Ra = 10^6$ with $\phi = 0.02$ whereas the corresponding increase is 6.52% for the case of without BM.

Nomenclature

B_0	MF strength [$Nm^{-1}A^{-1}$]	ave	Average
c_p	Specific heat [$Jkg^{-1}K^{-1}$]	bf	Base fluid
D_T	Thermal diffusion coefficient [m^2s^{-1}]	c	Cold
D_T^l	Numeric value of D_T	h	Hot
d_p	Diameter of nanoparticles [nm]	nf	nanofluid
Da	Darcy number	Greek symbols	
g	Gravitational acceleration [ms^{-2}]	δ	MF inclination angle [rad]
L	Cavity length[m]	λ	Dimensionless period number
Ha	Hartmann number	ρ	Density [kgm^{-3}]
		τ	Dimensionless time

κ	TC [$Wm^{-1}K^{-1}$]	ϕ	Volume fraction
k_B	Boltzmann constant [JK^{-1}]	ε	Porosity
K	Permeability (m^2)	α	Thermal diffusivity [m^2s^{-l}]
Nu	Nusselt number	μ	Dynamic viscosity [Nsm^{-2}]
p	Fluid pressure [Pa]	υ	Kinematic viscosity [m^2s^{-l}]
Pr	Prandtl number	σ	Electric conductivity [s/m]
Ra	Rayleigh number	θ	Dimensionless temperature
T	Fluid Temperature [K]	β	Thermal expansion coefficient [$1/K$]
T_{ref}	Reference temperature (K)	Abbreviations	
t	Dimensiona1 time [s]	BM	Brownian motion
u,v	Velocity components in x ,y directions [ms^{-1}]	PM	Porous medium
U,V	Dimensionless velocity components	HT	Heat transfer
x,y	Cartesian coordinates [m]	MF	Magnetic field
X,Y	Dimensionless coordinates	NP	Nanoparticle
Subscripts		NF	Nanofluid

Acknowledgements

The authors are obliged to the unspecified reviewers for their useful comments and suggestions for the further development of the paper. Md. Nurul Huda is also grateful to the MoST of Bangladesh for providing a doctoral fellowship of this research work.

References

Alam MS, Keya SS, Salma U, Hossain SMC, Billah MM. 2022. Convective heat transfer enhancement in a quarter-circular enclosure utilizing nanofluids under the influence of periodic magnetic field. Int. J. Thermofluids, 16: 100250.

Alam MS, Rahman MM, Parvin S and Vajravelu K. 2016. Finite element simulation for heat line visualization of natural convective flow and heat transfer inside a prismatic enclosure. Int. J. Heat Technol, 34(3): 391-400.

Al-Waheibi SM, Rahman MM, Sagir MZ. 2021. Free convective heat transmission under LTNE in nanofluids within a trapezoidal permeable crater in view of three energy equations: influences of variable permeability and porosity. Int. J. Thermofluid Science and Technology, 8(2): 080204.

Al Kalbani KS, Alam MS, Rahman MM. 2016. Finite Element Analysis of Unsteady Natural Convective Heat Transfer and Fluid Flow of Nanofluids inside a Tilted Square Enclosure in the Presence of Oriented Magnetic Field. American J. Heat and Mass Transfer, 3(3): 186-224.

Al-Zamily AMJ. 2014. Effect of magnetic field on natural convection in a nanofluid-filled semi-circular enclosure with heat flux source. Computers & Fluids, 103: 71-85.

Baytas AC, Pop I. 1999. Free convection in a oblique enclosures filled with a porous medium. Int. J. Heat and Mass Transfer, 42: 1047-1057.

Bear J. 1972. Dynamics of Fluids in Porous Media. Elsevier, New York.

Bejan A. 1987. Hand book of single-phase convective heat transfer. Wiley, New York.

Brinkman HC. 1947. On the permeability of media consisting of closely packed porous particles. Appl. Sci. Res. A 1: 81–86.

Celli M. 2013. Non-homogeneous model for a side heated square cavity filled with a nanofluid. Int. J. Heat Fluid Flow, 44: 327-355.

Choi SUS. 1995. Enhancing thermal conductivity of fluids with nanoparticles. In: Signier DA,

Wang HP (eds.) Development and applications of non-Newtonian flows. ASME FED,231(MD66): 99–105.

Ingham DB, Pop I. 2005. Transport Phenomena in Porous Media III. Elsevier, Oxford.

Izadi M, Sheremet MA, Mehryan SAM. 2020. Natural convection of hybrid nanofluid affected by an inclined periodic magnetic field within a porous medium. Chinese J. Physics, 65: 447-458.

Manole DM, Lage JL. 1992. Numerical benchmark results for natural convection in a porous medium cavity. Heat Mass Transfer Porous Media, 105: 44-59.

Mehryan SAM, Izadi M, Chamkha AJ, Sheremet MA. 2018. Natural convection and entropy generation of a ferrofluid in a square enclosure under the effect of a horizontal periodic magnetic field. J. Molecular Liquids, 263: 510-525.

Muskat M. 1946. The Flow of Homogeneous Fluids through Porous Media. Edwards, Michigan.

Nakayama A, Kokudai T, Koyama H. 1990. Non-Darcian boundary layer flow and forced convective heat transfer over a flat plate in a fluid-saturated porous medium. ASME J. Heat Transfer, 112: 157–162.

Nield DA, Bejan A. 2013. Convection in Porous Media. Springer, New York.

Rahman MM, Amir KA and Pop I. 2021. Darcy-Boussinesq convective flow in rectotrapezoidal enclosure with thermal stratification. J. Thermal Analysis and Calorimetry, 145: 3325-3337.

Rahman MM, Parvin S, Saidur R and Rahim NA. 2011. Magnetohydrodynamic mixed convection in a horizontal channel with an open cavity. Int. Commun. Heat and Mass Transfer, 38: 184–193.

Rahman MM, Alim MA and Mamun MAH. 2009. Finite element analysis of mixed convection in a rectangular cavity with a heat-conducting horizontal circular cylinder. Nonlinear Analysis: Modelling and Control, 14(2): 217-247.

Sheikholeslami M. 2018. CuO-water nanofluid flow due to magnetic field inside a porous media considering Brownian motion. Journal of Molecular Liquids, 249: 921-929.

Sheremet MA, Grosan T, Pop I. 2015. Free convection in a square cavity filled with a porous medium saturated by nanofluid using Tiwari and Das' nanofluid model. Transp. Porous Medium, 106: 595-610.

Siddiqa S, Faryad A, Begum N, Hossain MA, Gorla RSR. 2017. Periodic magnetohydrodynamic natural convection flow of a micropolar fluid with radiation. Int. J. Thermal Sci. 111: 215-222.

Tiwari RK, Das MK. 2007. Heat transfer augmentation in a two-sided lid-driven differentially heated square cavity utilizing nanofluids. Int. J. Heat and Mass Transfer, 50: 2002-2018.

Turcotte DL, Lyons JM. 2006. A periodic boundary-layer flow in magnetohydrodynamics. J. Fluid Mech, 13: 519-528.

Walker KL, Homsy GM. 1978. Convection in porous media. J. Fluid Mech, 87: 338-363.

Zienkiewicz OC and Taylor RL. 1991. The finite element method. 4th Edition, McGraw-Hill.